JOURNAL PRE-PROOF

This is an early version of the article, published prior to copyediting, typesetting, and editorial correction. The manuscript has been accepted for publication and is now available online to ensure early dissemination, author visibility, and citation tracking prior to the formal issue publication.

It has not undergone final language verification, formatting, or technical editing by the journal's editorial team. Content is subject to change in the final Version of Record.

To differentiate this version, it is marked as "PRE-PROOF PUBLICATION" and should be cited with the provided DOI. A visible watermark on each page indicates its preliminary status.

The final version will appear in a regular issue of *Engineering Transactions*, with final metadata, layout, and pagination.

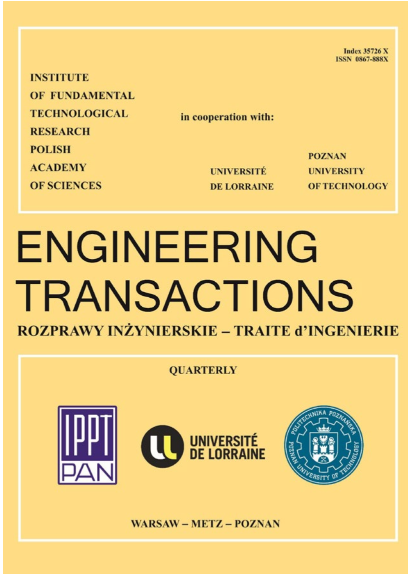

Title: Design, development, and testing of heat pipe evacuated tube solar collector using graphene oxide nanofluid

Author(s): Sumit Surve, RSN Sahai, Pravin Nana Jadhav

DOI: https://doi.org/10.24423/engtrans.2026.3645

Journal: *Engineering Transactions*

ISSN: 0867-888X, e-ISSN: 2450-8071

Publication status: In press

Received: 2025-08-29

Revised: 2026-05-11

Accepted: 2026-07-09

Published pre-proof: 2026-07-27

Please cite this article as:

Surve S., Sahai RSN, Jadhav P.N., Design, development, and testing of heat pipe evacuated tube solar collector using graphene oxide nanofluid, *Engineering Transactions*, 2026, https://doi.org/10.24423/engtrans.2026.3645

Copyright © 2026 The Author(s).
This work is licensed under the Creative Commons Attribution 4.0 International CC BY 4.0.

DESIGN, DEVELOPMENT, AND TESTING OF HEAT PIPE EVACUATED TUBE SOLAR COLLECTOR USING GRAPHENE OXIDE NANOFLUID

Sumit Surve[1], RSN Sahai[1] and Pravin Nana Jadhav[2*]

[1]General Engineering Department, Institute of Chemical Technology, Mumbai, India.
[2]Mechanical Engineering Department, Gharda Institute of Technology, Ratnagiri, India,

Email Ids:1. **Sumit Surve-** sssurve1987@gmail.com, **2. RSN Sahai-** rsn.sahai@ictmumbai.edu.in, 3. **Pravin Nana Jadhav-**pnjadhav@git-india.edu.in

*Corresponding Author: **Pravin Nana Jadhav-** pnjadhav@git-india.edu.in

ABSTRACT:

This study investigates the design and performance of a heat pipe-based evacuated tube solar collector (ETSC) incorporating a copper coil heat exchanger and graphene oxide (GO)-deionized (DI) water nanofluids. Nanofluid samples with GO concentrations of 0.0015% and 0.0025% by volume were synthesized and tested at mass flow rates of 0.5 L/min and 1 L/min. Stability analysis using zeta potential measurements confirmed that the nanofluids remained stable for up to 40 days. The experimental tests, conducted at Ratnagiri, Maharashtra (Latitude: 17.05°N; Longitude: 73.56°E), demonstrated significant enhancements in heat gain and temperature differentials when GO/DI nanofluids were used compared to conventional water. Thermal efficiency improved with increasing nanofluid concentration and flow rate, achieving a maximum relative enhancement in thermal efficiency of 28.2% compared to water at a concentration of 0.0025% and a flow rate of 1 L/min. These findings highlight the potential of GO/DI nanofluids to enhance the thermal performance of ETSCs, providing a promising approach for improving solar energy utilization. The results demonstrate that GO/DI nanofluids can significantly enhance ETSC performance with minimal cost implications, making them a promising solution for efficient solar thermal systems.

Keywords: Evacuated tube, Solar collector, Graphene oxide, Thermal performance

1. INTRODUCTION

In the modern era of rapid development, the growing energy demand poses a significant challenge to meet requirements without causing environmental harm. With the depletion of conventional energy resources, researchers are actively exploring alternative solutions. Renewable energy has emerged as a promising option due to its abundance and environmental friendliness. Among these, solar energy can be harnessed through two primary methods: (a) photovoltaic cells that convert solar heat into electricity and (b) solar thermal systems employing solar collectors.

Enhancing the thermal performance of solar collectors has been a focus of research, with nanofluids frequently employed as advanced working fluids [1]. Nanofluids are engineered by

PRE-PROOF PUBLICATION

PRE-PROOF PUBLICATION ENGINEERING TRANSACTIONS

dispersing nanoparticles, typically metals or metal oxides with diameters less than 100 nm, in a base fluid like water, which enhances heat transfer properties. Conventional water-based working fluids in solar collectors often result in lower thermal efficiency, as noted in earlier studies [2]. While system redesigns can improve efficiency, they often incur higher costs. Hence, the use of nanofluids offers a potentially effective approach for enhancing thermal performance, particularly when used at low concentrations where implications cost remains limited. Yousefi et al. [3] investigated the impact of aluminum oxide (Al_2O_3)-water nanofluids at volume fractions of 0.03% and 0.06% and flow rates ranging from 20 to 60 L/hr on an evacuated tube solar collector (ETSC), achieving notable efficiency improvements. Another study on water nanofluids demonstrated a 50% increase in heat energy and output temperature with varying mass flow rates and concentrations [4]. Similarly, research on silver-water nanofluids in a thermosyphon heat pipe ETSC revealed an efficiency increase from 20.7% to 40% compared to water alone [5].

Additional experiments employing single-walled carbon nanotubes (SWCNTs) in water-based nanofluids assessed the ETSC's performance at volume fractions of 0.05%, 0.1%, and 0.2% under various flow rates. Results indicated that a 0.2% concentration achieved a peak thermal efficiency of 93.43% [6]. Moreover, copper-water nanofluids were found to deliver superior heat recovery and reduce emissions of carbon dioxide (CO_2) and sulfur dioxide (SO_2). Experimental and numerical analyses, including finite element analysis (FEA), of nanofluids such as MWCNTs, TiO_2, SiO_2, and C_u with water as the base fluid, further validated the enhanced performance of ETSCs [7].

Table 1. Thermal conductivity of different materials

			Thermal Conductivity (W/m.k)
1.	Base fluids	Water	0.613
		Ethylene glycol	0.253
2.	Metallic solids	Silver	429
		Copper	401
3.	Non-metallic solids	Graphene	~ 3000 - 5000

The primary objective of this research is to enhance the thermal performance of an evacuated tube solar collector (ETSC) by utilizing graphene oxide (GO) nanoparticles in a deionized (DI) water-based nanofluid. GO nanoparticles were selected for their superior thermal conductivity, which plays a crucial role in efficient heat transfer and improving the performance of solar collectors. Previous studies, such as those by Ghosh and associates (2008), have explored the thermal performance of ETSCs using graphene nanoplatelets and methanol-based nanofluids [8], [9]. These investigations also evaluated the influence of parameters such as solar panel tilt angles, filling ratios, and flow rates on thermal efficiency. Building on this, Iranmanesh et al. examined ETSCs with graphene nanoplatelets in distilled water at concentrations of 0.025, 0.05, 0.075, and 0.1 wt.% and mass flow rates of 0.5 L/min, 1 L/min, and 1.5 L/min [10]. Their findings revealed a significant improvement in thermal efficiency, reaching up to 90.7% at a mass flow rate of 1.5 L/min compared to conventional water-based systems.

PRE-PROOF PUBLICATION

PRE-PROOF PUBLICATION ENGINEERING TRANSACTIONS

The novelty of this study lies in the integration of graphene oxide nanofluids with a heat pipe-based ETSC system incorporating a copper coil heat exchanger, along with experimental evaluation under practical operating conditions.

2. NOMENCLATURE

Symbol	Description	Units
A_c	Collector area	m²
C_p	Specific heat of fluid	J/kg.K
d_i	Inner diameter of tube	mm
d_o	Outer diameter of tube	mm
D_e	Equivalent diameter	mm
G	Solar radiation	W/m²
h_i	Inner heat transfer coefficient	W/m².K
h_o	Outer heat transfer coefficient	W/m².K
k	Thermal conductivity	W/m.K
m	Mass flow rate	kg/s
N_{RE}	Reynolds number	–
N_{PR}	Prandtl number	–
Q_u	Useful heat gain	W
T_i,T_o	Inlet and outlet temperatures	°C
μ	Dynamic viscosity	Pa.s
μ_w	Dynamic viscosity at wall temperature	Pa.s
ρ	Density	kg/m³
η	Thermal efficiency	–

3. EXPERIMENTAL PROCEDURES

All materials and instruments used for the fabrication and measurement of the test setup were selected in accordance with BIS and ASHRAE standards for solar water heating systems.

3.1. Synthesis of Graphene Oxide

The GO nanomaterial was synthesized in the laboratory using an improved, widely adopted method for large-scale GO production, which is both efficient and safe [11].

PRE-PROOF PUBLICATION
PRE-PROOF PUBLICATION ENGINEERING TRANSACTIONS

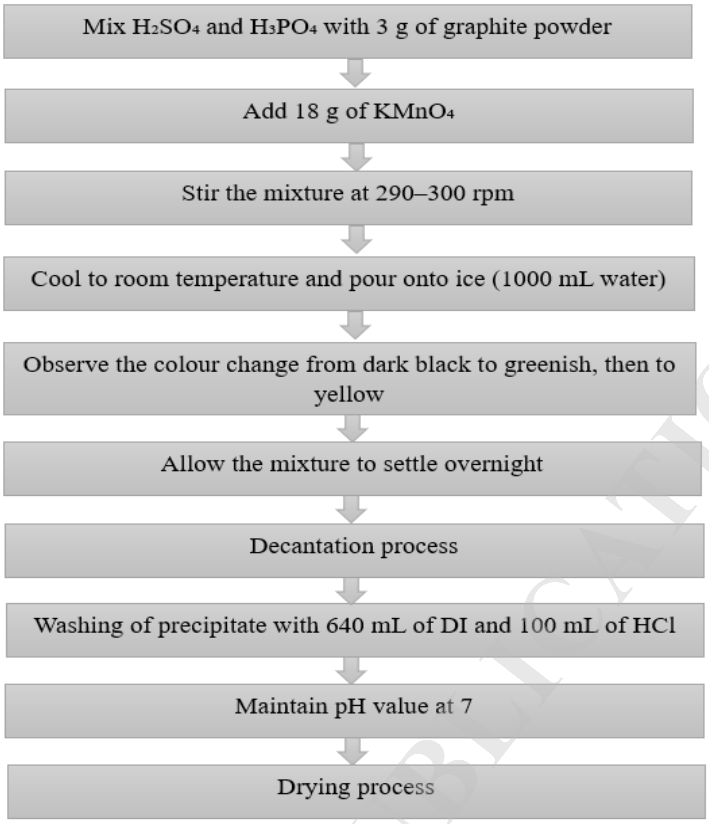

Figure 1. Flowchart for Enhanced Graphene Oxide (GO) Synthesis Method.

The required amount of GO was accurately measured using a precision weighing machine and dispersed in deionized (DI) water. The mixture was then subjected to ultrasonication, resulting in the preparation of GO/DI nanofluids with volumetric concentrations of 0.0015% and 0.0025%.

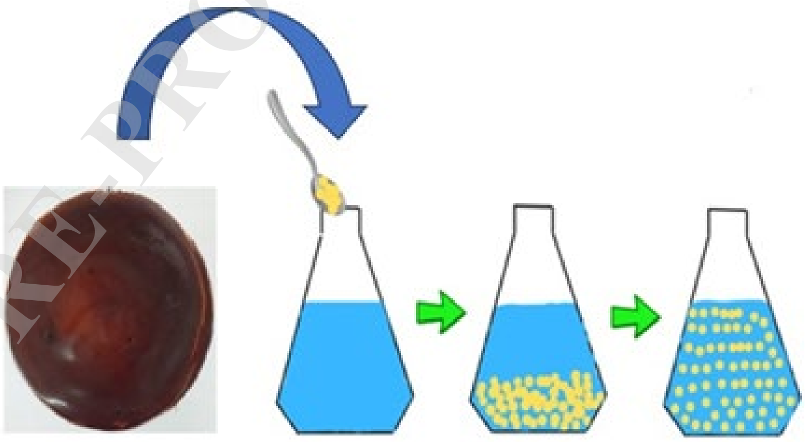

Figure 2. Graphene Oxide Nanomaterial Synthesis.

3.2. Stability of Nanofluid

A key challenge in nanofluid fabrication is ensuring its stability, making stability assessment a critical step before testing in collectors [12]. While several techniques are available for evaluating nanofluid stability, zeta potential analysis is the most commonly used method. In this study, the zeta potential of the nanofluid samples was measured immediately after

PRE-PROOF PUBLICATION ENGINEERING TRANSACTIONS
PRE-PROOF PUBLICATION

preparation, and the samples were observed over a 40-day period to assess their stability.

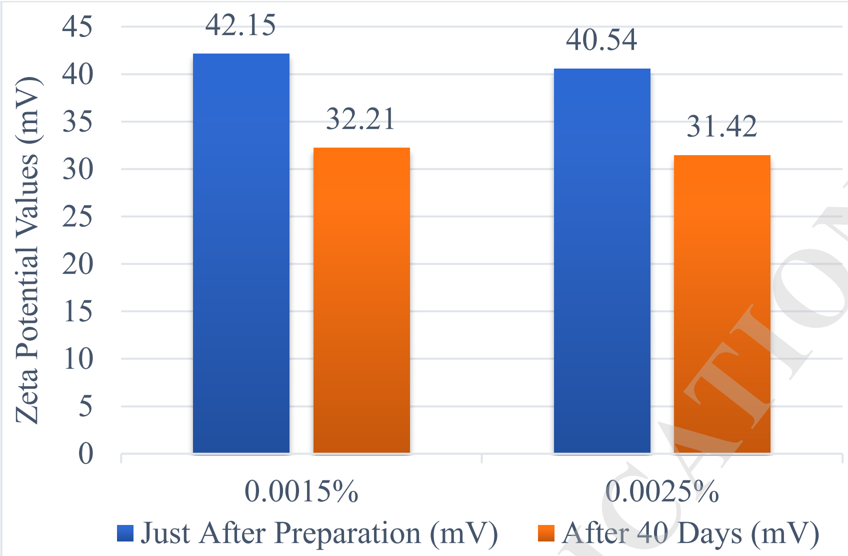

Figure 3. Stability Analysis of GO/DI Nanofluid Samples.

Based on Figure 3, it can be concluded that the samples remain stable for up to 40 days. Zeta potential values ranging from ±40 to ±60 mV indicate good stability, while values between ±30 to ±40 mV confirm the stability of the nanofluid solution [13].

3.3. Design of copper coil heat exchanger

Heat exchange between flowing fluids is one of the most critical physical processes. The primary objective of designing a heat exchanger is to efficiently transfer heat from one fluid to another, either directly or indirectly. Helical coils with circular cross-sections are commonly used in various applications due to their ease of manufacture [14].

Table 2. Heat exchanger designed parameters.

Dimensional parameter	**Dimension (mm)**
1. Tube inner diameter (d_i)	10
2. Tube outer diameter (d_o)	12.5
4. Mean coil diameter (D_h)	250
5. Pitch (P)	60
6. No of turns (N)	8

1. The total length of coil (L), needed for number of turns:

$$L = N\sqrt{(2\pi r)^2 + P^2} \quad (1)$$

Where,

r =D_h/2 is the mean radius of the coil (mm),

Pis the pitch of the coil (mm),

N is the number of turns.

PRE-PROOF PUBLICATION
PRE-PROOF PUBLICATION ENGINEERING TRANSACTIONS

The calculated length of the coil is:

L= 6301.49 mm

2. The volume occupied by the coil (V_c):

$$Vc = \frac{\pi}{4} \; d_o^2 L \qquad (2)$$

Where,
d_o is the outer diameter of the tube (mm),
L *is the length of the coil (mm).*

V_c= 773309.16 mm^3

3. Volume of annulus (V_a):

$$V_a = \frac{\pi}{4} \left(D_o{}^2 - D_i{}^2\right)P.N \qquad (3)$$

Where,
D_o is the outer diameter of the shell (mm),
D_i is the inner diameter of the shell (mm),
P is the pitch (mm),
N is the number of turns.

V_a = 9424777.96 mm^3

4. The volume that is accessible for fluid flow in the annulus (V_f)

$$V_f = V_a - V_c \qquad (4)$$

= 8651468.8 mm^3

5. Equivalent diameter of a coiled tube on the shell side (D_e):

$$D_e = \frac{4.V_f}{\pi.d_o.L} \qquad (5)$$

Where,
V_f is the effective flow volume (mm^3),
d_o is the outer diameter of the tube (mm),
L is the coil length (mm).

6. The heat transfer coefficient in the annulus (h_o):

If, The Reynolds number (N_{RE}) is in the range of 50-10,000 then,

$$\frac{h_o.D_e}{k} = 0.6\, N_{RE}{}^{0.5}.N_{PR}{}^{0.31} \qquad (6)$$

7. If Reynolds number (N_{RE}) is greater than 10,000 then,

$$\frac{h_o.D_e}{k} = 0.36\, N_{RE}{}^{0.55}.N_{PR}{}^{0.33}.\left(\frac{\mu}{\mu w}\right)^{0.14} \qquad (7)$$

Where,
h_o is the convective heat transfer coefficient on the annulus side (W/m^2. K),
μw is the dynamic viscosity at wall temperature (Pa·s).

8 Reynolds number (N_{RE}), can be expressed as,

PRE-PROOF PUBLICATION
PRE-PROOF PUBLICATION ENGINEERING TRANSACTIONS

$$N_{RE} = \frac{\rho V d_o}{\mu} \quad (8)$$

9. Also, Prandtl numbers (N_{PR}) are calculated as,

$$N_{PR} = \frac{\mu . C_p}{k} \quad (9)$$

Where,
ρ is the fluid density (kg/m^3),
V is the fluid velocity (m/s), as compared to water
μ is the dynamic viscosity of fluid (Pa·s),
C_p is the specific heat of fluid (J/kg·K),
k is the thermal conductivity (W/m·K).

By calculating,

N_{RE}= 467 < 10,000 (Laminar flow)

N_{PR} = 12.51

Heat transfer coefficient in annulus,

(h_o) = 478 W/m. k

Similarly,

10. Heat transfer coefficient of fluid flowing inside the coil (h_i) can be calculated in the same manner,

$$(H_{i.} D_e/k) = 0.6 \, N_{RE}^{0.5} . N_{PR}^{0.31} \quad (10)$$

Putting all the values we will get,

N_{RE} = 588 < 2,300 (Laminar flow)

N_{PR}= 12.51

Therefore, h_i= 656 W/m.k

Figure 4. Fabricated copper coil heat exchanger.

PRE-PROOF PUBLICATION
PRE-PROOF PUBLICATION ENGINEERING TRANSACTIONS

3.4 Sensors and temperature indicator

K-type thermocouples are known for their wide operating temperature range. They consist of a non-magnetic positive leg and a magnetic negative leg. Due to the use of traditional base metals, K-type thermocouples are capable of operating at high temperatures and offer a broad temperature range [15].All these sensors were connected to a temperature indicator (8 channels) to measure temperature at respective locations.

Figure 5. Thermocouple and temperature indicator.

3.5. Safety valves

3.5.1. Two-way ball valves

In order to remove and refill the corresponding working fluid to the system, the two-way ball valve made up of brass was used. Similarly, these two-way ball valves act as a safety device for the experimental test setup.

Figure 6. Pictures of two-way ball valves.

3.5.2. Pressure relief valve (PRV)

A safety valve known as a pressure relief valve (PRV) is used to regulate or control the pressure

PRE-PROOF PUBLICATION
PRE-PROOF PUBLICATION ENGINEERING TRANSACTIONS

in a system. Otherwise, pressure will rise in the system and cause a system failure or fire. This pressure is removed from the system by allowing the pressurized fluid to flow out of the system through an auxiliary passage [16].

Figure 7. Installed pressure relief valve.

3.5.3. Air relief valve

Air relief valves, also known as air release valves or air valves, serve as a safety mechanism by venting air pockets that may form at high points in a fully pressurized system. If not released, these trapped air pockets can cause various issues, including flow disruptions, pump failures, corrosion, inaccurate instrument readings, and pressure surges [17].

Figure 8. Air relief valve.

3.6 Hot water pump

Centrifugal pumps are commonly recommended for use in solar water heating systems. Additionally, a positive displacement pump equipped with a relief valve is advised, especially when testing with oil or hydrocarbons (high-micron liquids) in the loop. In this experimental

PRE-PROOF PUBLICATION ENGINEERING TRANSACTIONS
PRE-PROOF PUBLICATION

setup, a Wilo-based hot water pump is utilized to circulate the working fluid under pressure within the solar system. The pump offers variable flow settings of 0.5 L/min, 0.75 L/min, and 1 L/min, eliminating the need for a separate fluid flow meter and its associated accessories for measurement.

Figure 9. Variable flow hot water pump.

3.7. Evacuated tube with heat pipe

The heat pipe, similar to a solar tube, consists of a hollow tube with an evacuated interior. The primary objective here is to alter the internal liquid state rather than providing insulation. A small amount of water or special additives is contained within the heat pipe. While water boils at 100°C (212°F) at sea level, its boiling point decreases with increasing altitude [18]. By evacuating the heat pipe, the boiling point of water is lowered, allowing the same outcome to be achieved at lower temperatures. In solar collector applications, the boiling point of the heat pipe is reduced to 30°C (86°F). As the heat pipe is heated above this temperature, the water inside vaporizes. The resulting vapor quickly rises to the top of the heat pipe, where it transfers heat. As the vapor loses heat at the condenser, it condenses back into liquid form, which then travels back to the bottom of the heat pipe [19].

PRE-PROOF PUBLICATION
PRE-PROOF PUBLICATION ENGINEERING TRANSACTIONS

Figure 10. Installation of evacuated tubes at the testing site.

3.8. Insulation materials and Storage tank

Thermal insulation offers several advantages, including preventing heat loss, reducing energy consumption, and lowering air-conditioning operating costs. By enhancing thermal insulation, the amount of heat gained is minimized, which leads to reduced energy usage [20]. In colder climates, heat tends to transfer from the interior to the exterior, making it essential to place the insulating layer on the inside of surfaces to minimize heat loss.

A storage tank is used to retain high-temperature water in solar water heating systems. These tanks typically have a capacity to hold 1.5 to 2 times the daily hot water demand. Tanks are made from materials such as copper, steel, or aluminum, but the inner lining must be made of a non-corrosive material that does not contaminate the water, especially in direct systems, and remains stable at specified operating temperatures. To promote stratification in thermosyphon systems, the hot water outlet pipe is positioned near the top of the tank [21].

To ensure efficient thermal retention, the temperature of the hot water should not decrease by more than 8°C over 16 hours. As a result, proper insulation is crucial. Insulation materials like fiberglass or cork, typically with a thickness of 7 to 10 cm, are recommended for solar water heating systems to maintain optimal performance [22].

3.9. Fabrication of experimental test set-up

The experimental test setup was fabricated and tested at the solar site in Ratnagiri, Maharashtra (Lat. 17.05° N; Long. 73.56° E), with a 40° tilt angle, oriented towards the south.

Table 3. Specification of ETSC

Parameters	**Dimension**
1. Diameter of tube	58 mm
2. Length of tube	1800 mm
3. Aperture area	1.92 m^2
4 No of Tubes	20 Nos
5. Tube wall thickness	1.6 mm

PRE-PROOF PUBLICATION ENGINEERING TRANSACTIONS

PRE-PROOF PUBLICATION

6. Absorber area	1.65 m^2
7. Stable vaccum	0.005 Pa

Figure 11 illustrates the closed-loop experimental test setup used to evaluate the thermal performance of the ETSC. The ETSC is connected to the system via a corrugated steel pipe, which includes both an inlet and an outlet. A temperature sensor is installed at the inlet to measure the temperature of the incoming fluid, while another sensor is placed at the outlet to monitor the temperature of the fluid leaving the collector.

Pressure gauges are positioned at both the entry and exit points of the collector to measure the pressure drop of the testing fluid. A flow meter is mounted to measure the mass flow rate, with a hot water pump installed before the flow meter to supply the necessary motive force, ensuring fluid circulation under pressure. A bypass valve is located on the discharge side of the pump to adjust the mass flow rate and prevent backpressure buildup in the system. As the hot water pump circulates the cold fluid through the system, the fluid passes through the collector, absorbs heat from the solar radiation incident on the ETSC, and becomes heated.

Figure 11. Fabricated ETSC test set up.

The heated fluid then enters the heat exchanger, where it transfers heat to the water inside the tank. As a result, the temperature of the water in the tank increases, while the cooled fluid is returned to the system for recirculation.

3.9.1. Thermal efficiency calculations

The useful heat gain (Qu) is calculated as,

$$Q_u = m.C_p.(T_o - T_i) \quad (11)$$

The heat gain by fluid also written as,

$$Q_u = A_C.F_R.[G\,(T_a) - U_L\,(T_i - T_a)] \quad (12)$$

Total input energy on ETSC is,

$$Q_{in} = A_c.G \quad (13)$$

Thermal efficiency is calculated by,

$$\eta = \frac{m.C_p.(T_o - T_i)}{A_c.G} = \frac{Q_u}{Q_{in}} * 100 \quad (14)$$

PRE-PROOF PUBLICATION ENGINEERING TRANSACTIONS

For quantitative comparison, the relative enhancement in thermal efficiency is defined as follows:

The relative enhancement in thermal efficiency is calculated as:

$$\text{Enhancement}(\%) = \frac{\eta_f - \eta_{water}}{\eta_{water}} * 100 \quad (15)$$

Where:
η_f is the thermal efficiency of the nanofluids-based system (%),
η_{water} is the thermal efficiency of the water-based (baseline) system (%).

4. RESULTS AND DISCUSSION

Initially, water was used as the working fluid in the ETSC setup, followed by testing with nanofluid samples, and the results were recorded. Solar radiation was measured using a pyranometer, while wind speed was monitored with an anemometer. The tests were conducted from 9:30 AM to 4:30 PM, with readings taken every 30 minutes. Four sensors were used during the experiment to measure temperatures at various locations:

a. Inlet Temperature Sensor (T1)**:** Measures the temperature of the incoming fluid to the ETSC manifold.
b. Outlet Temperature Sensor (T2)**:** Measures the temperature of the fluid leaving the ETSC manifold.
c. Water Tank Temperature Sensor (T3)**:** Measures the temperature of the water inside the tank.
d. Ambient Temperature Sensor (T4)**:** Measures the ambient temperature.

4.1. Effect of solar radiations

Figure 12 illustrates the variation in solar radiation absorbed by the collector and the ambient temperature data recorded during the test period from 9:30 AM to 4:30 PM. The graph indicates that solar radiation increases with time, peaking around 1:00 PM, after which it begins to decline. The trend follows a parabolic pattern, and similar graphical trends for solar radiation were observed across all test readings.

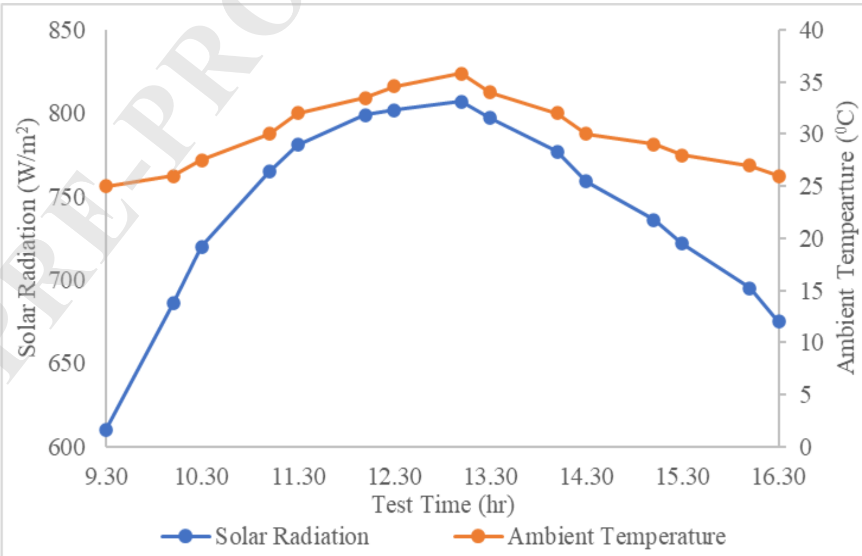

Figure 12. Solar radiation, ambient temperature data versus test time.

Based on Figure 12, the maximum solar radiation absorbed was recorded between 12:00 PM and 1:30 PM, with a peak value of 807 W/m² at 1:00 PM. This highlights a direct relationship

PRE-PROOF PUBLICATION ENGINEERING TRANSACTIONS
PRE-PROOF PUBLICATION

between solar radiation and input energy, with higher input energy observed around noon compared to the pre-noon and post-noon periods. The ambient temperature also exhibited an increasing trend throughout the test period, reaching its highest value at 1:00 PM.

4.2. Temperature difference

Temperature difference is a crucial parameter in evaluating the performance of thermal collectors, as it is directly proportional to their thermal efficiency. For water as the working fluid, a temperature difference of 6.2°C was observed at a mass flow rate of 0.5 L/min, which decreased to 5.5°C as the mass flow rate increased to 1 L/min. Similarly, for a volumetric concentration of 0.0015% GO/DI nanofluid, the temperature differences were recorded as 7.6°C and 6.9°C at mass flow rates of 0.5 L/min and 1 L/min, respectively.

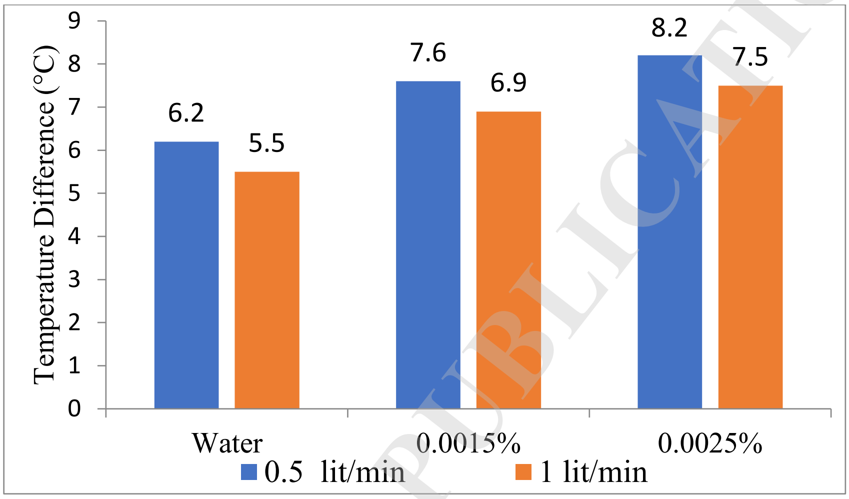

Figure 13. Maximum temperature difference values of working samples.

The highest temperature differences were observed for a volumetric concentration of 0.0025%, recorded as 8.2°C and 7.5°C at mass flow rates of 0.5 L/min and 1 L/min, respectively. This increase in temperature difference can be attributed to the superior thermal conductivity of graphene oxide compared to water, which enhances the overall thermal conductivity of the nanofluid samples. Consequently, this improved thermal conductivity leads to an increase in the overall heat transfer coefficient of the nanofluid samples [23, 24].

4.3. Water temperature inside the tank

The circulation of nanofluid through the ETSC facilitates heat exchange with the water inside the tank via a copper coil heat exchanger, resulting in an increase in the tank water temperature. These recorded values are presented in Figure 14 below.

PRE-PROOF PUBLICATION

PRE-PROOF PUBLICATION ENGINEERING TRANSACTIONS

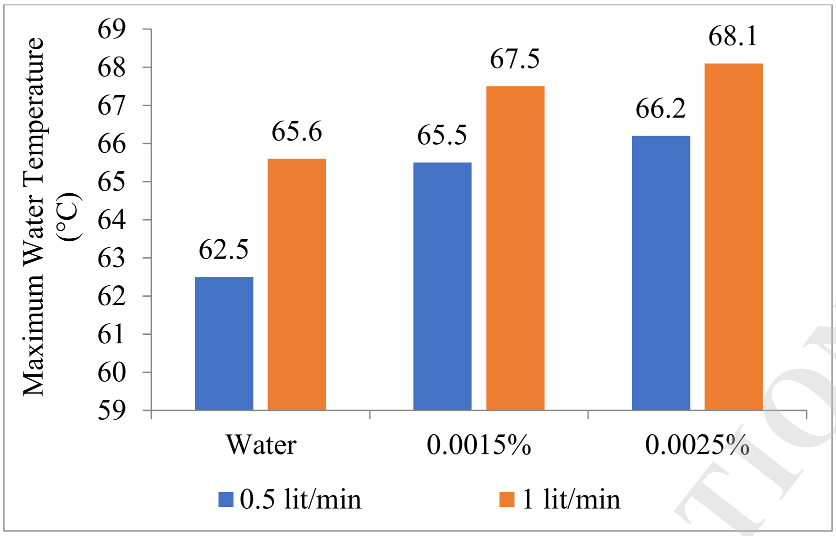

Figure 14. Temperature of water inside the tank versus working fluid samples.

The water tank temperature rises with an increase in the mass flow rate and volumetric concentration of the nanofluid. At a mass flow rate of 0.5 L/min and 1 L/min, the maximum water temperatures were recorded as 62.5°C and 65.6°C, respectively. These values increased to 65.5°C and 67.5°C for a volumetric concentration of 0.0015% at the same mass flow rates. The highest water temperatures were observed at the higher volumetric concentration of 0.0025%. This increase in water temperature is attributed to the combined effects of higher mass flow rates and temperature differences, which are directly proportional to the heat gain by the fluid. Consequently, increased volumetric concentrations and mass flow rates enhance the energy absorption, leading to higher water temperatures inside the tank [25].

4.4. Thermal Efficiency

The thermal efficiency of the ETSC using water and GO/DI nanofluid samples was analyzed at mass flow rates of 0.5 L/min and 1 L/min, as depicted in Figures 15 and 16. The thermal efficiency of both water and nanofluid samples increased with time during the test, reaching its peak at 1:00 PM for all samples. After 1:00 PM, the thermal efficiency began to decline as time progressed. This variation in thermal efficiency is directly influenced by the values of absorbed solar radiation.

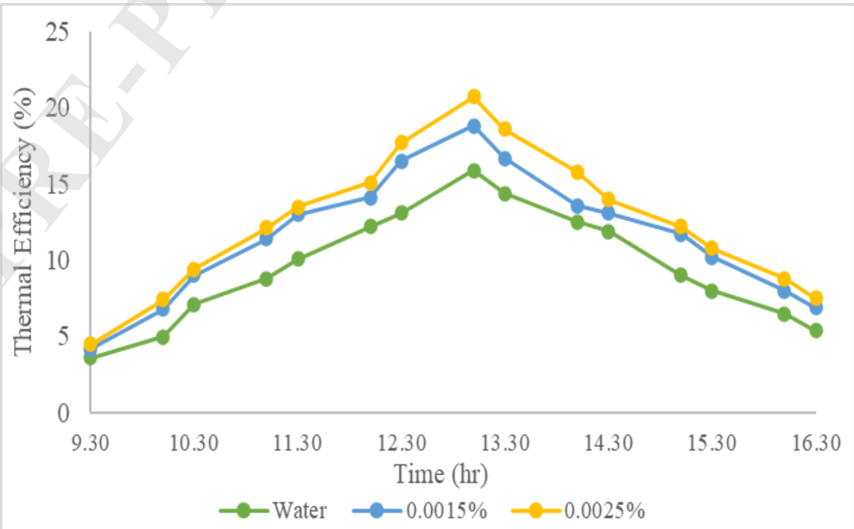

Figure 15. Variation of thermal efficiency of water and GO/DI nanofluid samples at a mass flow rate of 0.5 L /min.

PRE-PROOF PUBLICATION
PRE-PROOF PUBLICATION ENGINEERING TRANSACTIONS

The maximum thermal efficiency for water was recorded as 15.9% at 1:00 PM with a mass flow rate of 0.5 L/min. This efficiency increased with higher volumetric concentrations and mass flow rates. For a volumetric concentration of 0.0015%, the thermal efficiency reached 18.8% at a mass flow rate of 0.5 L/min. As the mass flow rate increased, the thermal efficiency of the ETSC also improved, with the highest efficiency observed at a volumetric concentration of 0.0025% and a mass flow rate of 1 L/min.

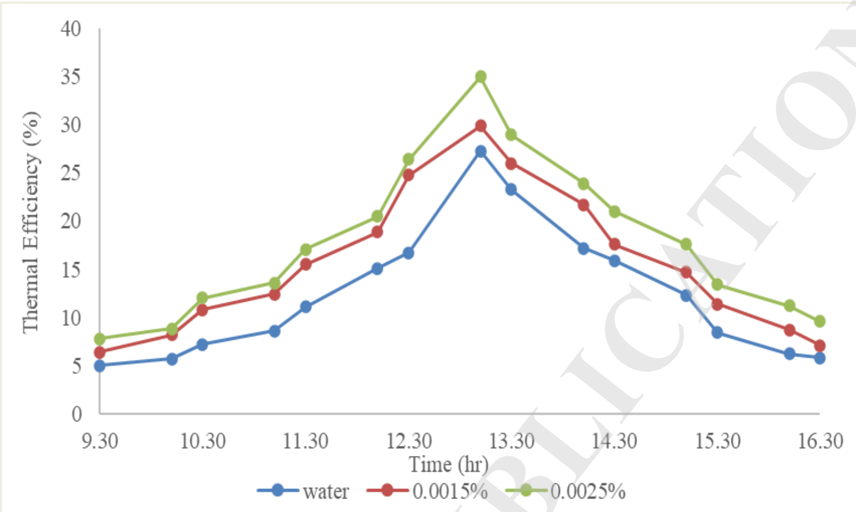

Figure 16. Variation of thermal efficiency with time for water and GO/DI nanofluid samples at a mass flow rate of 1 L /min.

The maximum relative enhancement in thermal efficiency of the ETSC was found to be 28.2% compared to water, calculated based on the percentage increase from the baseline water efficiency by using volumetric concentration of 0.0025% as compare to water. The efficiency increment is defined as the relative percentage increase in thermal efficiency of the nanofluid system compared to the water-based system.

Table 4. Thermal efficiency vs mass flow rate

Samples	**Thermal efficiency (%)**	**Mass flow rate**	
		0.5 L/min	**1 L/min**
Water	Maximum	15.9	27.3
	Average	9.6	12.4
0.0015%	Maximum	18.8	29.9
	Average	11.6	15.6
0.0025%	Maximum	20.7	35
	Average	12.6	17.8

In addition to thermal performance, the economic feasibility of nanofluid application is an important consideration. Although nanofluids are relatively more expensive than water, the present study utilizes graphene oxide (GO) at a very low volumetric concentration of 0.0025%, thereby minimizing the additional material cost. The thermal efficiency increases from 27.3% for water to 35% for the nanofluid, corresponding to a relative enhancement of 28.2%. Similar

PRE-PROOF PUBLICATION
PRE-PROOF PUBLICATION ENGINEERING TRANSACTIONS

improvements in heat transfer performance using nanofluids have been reported in previous studies [4, 26, 3]. The enhanced efficiency leads to higher heat gain and faster water heating, which can reduce the dependence on auxiliary energy sources. Over time, the associated energy savings can compensate for the initial additional cost, indicating that the use of GO/DI nanofluids offers a practical and economically viable approach for improving solar collector performance.

It should be noted that the present study is limited to short-term experimental evaluation under specific climatic conditions, and long-term stability and large-scale economic analysis require further investigation.

CONCLUSIONS

The experimental investigation of the heat pipe evacuated tube solar collector (ETSC) utilized GO/DI water nanofluid. Following preparation, the stability of the GO/DI water nanofluid was assessed and found to remain stable without sedimentation for up to 40 days. The ETSC test setup was employed to evaluate pure water and GO/DI water nanofluid samples with volumetric concentrations of 0.0015% and 0.0025% at mass flow rates of 0.5 L/min and 1 L/min, respectively. Key thermal performance metrics, including thermal efficiency, useful heat gain, and temperature difference, were analyzed. The highest water temperature in the storage tank (68.1°C) and the maximum thermal efficiency of the ETSC (35%) were achieved at a volumetric concentration of 0.0025% and a mass flow rate of 1 L/min. This corresponds to a relative enhancement of 28.2% in thermal efficiency compared to the baseline water-based system under identical operating conditions. Therefore, graphene oxide-based nanofluids demonstrate strong potential for enhancing the thermal performance of evacuated tube solar collectors for sustainable solar thermal applications.

AKNOWLEDGMENT

The author would like to acknowledge the kind support and guidance received from the Department of Physics, Institute of Chemical Technology, Mumbai.

REFERENCES

[1] Ahmed A., Baig H., Sundaram S., Mallick T.K., Use of nanofluids in solar PV/thermal systems, *International Journal of Photoenergy*, **2019**: 1–17, 2019. DOI:10.1155/2019/8039129

[2] Kadhim S., Ibrahim O., Improving the thermal efficiency of flat plate solar collector using nano-fluids as working fluids: A review, *Iraqi Journal of Industrial Research*, **8**, 2021.

DOI:https://doi.org/10.53523/ijoirVol8I3ID86

[3] Yousefi T., Veysi F., Shojaeizadeh E., Zinadini S., An experimental investigation on the effect of Al_2O_3–H_2O nanofluid on the efficiency of flat-plate solar collectors, *Renewable Energy*, **39**(1): 293–298, 2012. DOI: https://doi.org/10.1016/j.renene.2011.08.056.

[4] Zhang X.R., Yamaguchi H., An experimental study on evacuated tube solar collector using supercritical CO_2, *Applied Thermal Engineering*, **28**(11–12): 1225–1233, 2008. DOI: https://doi.org/10.1016/j.applthermaleng.2007.07.013

[5] Ozsoy A., Corumlu V., Thermal performance of a thermosyphon heat pipe evacuated tube solar collector using silver-water nanofluid for commercial applications, *Renewable Energy*,

PRE-PROOF PUBLICATION

PRE-PROOF PUBLICATION ENGINEERING TRANSACTIONS

122: 26–34, 2018. DOI: https://doi.org/10.1016/j.renene.2018.01.031

[6] Sabiha M.A., Saidur R., Hassani S., Said Z., Mekhilef S., Energy performance of an evacuated tube solar collector using single-walled carbon nanotube nanofluids, *Energy Conversion and Management*, **105**: 1377–1388, 2015. DOI: https://doi.org/10.1016/j.enconman.2015.09.009

[7] Yurddaş A., Optimization and thermal performance of evacuated tube solar collector with various nanofluids, *International Journal of Heat and Mass Transfer*, **152**: 119496, 2020. DOI: https://doi.org/10.1016/j.ijheatmasstransfer.2020.119496

[8] Ghosh S., Calizo I., Teweldebrhan D., Pokatilov E.P., Nika D.L., Balandin A.A., Bao W., Miao F., Lau C.N., Extremely high thermal conductivity of graphene: Prospects for thermal management applications in nanoelectronic circuits, *Applied Physics Letters*, **92**(15): 151911, 2008. DOI: https://doi.org/10.1063/1.2907977.

[9] Sarafraz M.R., Safaei M.R., Diurnal thermal evaluation of an evacuated tube solar collector charged with graphene nanoplatelets–methanol nanosuspension, *Renewable Energy*, **142**: 364–372, 2019. DOI: https://doi.org/10.1016/j.renene.2019.04.091

[10] Iranmanesh S., Ong H.C., Ang B.C., Sadeghinezhad E., Esmaeilzadeh A., Thermal performance enhancement of an evacuated tube solar collector using graphene nanoplatelets nanofluid, *Journal of Cleaner Production*, **162**: 121–129, 2017. DOI: https://doi.org/10.1016/j.jclepro.2017.05.175

[11] Al-Ruqeishi M., Mohiuddin T., Al-Moqbali M., Al-Hinai M., Graphene oxide synthesis: Optimizing the Hummers and Marcano methods, *Nanoscience and Nanotechnology Letters*, **12**(1): 88–95, 2020. DOI: 10.1166/nnl.2020.3074

[12] Ali A.R.I., Salam B., A review on nanofluid: Preparation, stability, thermophysical properties, heat transfer characteristics and applications, *SN Applied Sciences*, **2**: 1636, 2020. DOI: https://doi.org/10.1007/s42452-020-03427-1

[13] Chang H., Jwo C., Fan P., Pai S., Process optimization and material properties for nanofluid manufacturing, *International Journal of Advanced Manufacturing Technology*, **34**(3–4): 300–306, 2007. DOI: https://doi.org/10.1007/s00170-006-0597-0

[14] Titus A.K., Fareedudeen K., Ahmed K.S., Sabarish Kumar P., Sreejith K., Design and analysis of helical coil heat exchanger, *IOP Conference Series: Materials Science and Engineering*, **923**: 012016, 2020. DOI: https://doi.org/10.1088/1757-899X/923/1/012016.

[15] Tucker D.J.L., Edler F., Žužek V., Broughton K.J., Thermoelectric stability of dual-wall and conventional Type K and N thermocouples, *Measurement Science and Technology*, **33**(7): 075003, 2022. DOI: https://doi.org/10.1088/1361-6501/ac57ee

[16] Anwar A.A., Gorash Y., Dempster W., Hamilton R., Literature research in relevant fields to understand pressure relief valve leak tightness in a static closed state, *Procedia Engineering*, **130**: 95–103, 2015. DOI: https://doi.org/10.1016/j.proeng.2015.12.179

[17] Thapa P., Design and calculation of the pressure relief valves and rupture disks system, *IOP Conference Series: Materials Science and Engineering*, **888**: 013016, 2020. DOI: https://doi.org/10.13140/RG.2.2.18443.90403

PRE-PROOF PUBLICATION

PRE-PROOF PUBLICATION ENGINEERING TRANSACTIONS

[18] Shukla R., Sumathy K., Erickson P., Gong J., Recent advances in solar water heating systems: A review, *Renewable and Sustainable Energy Reviews*, **19**: 173–190, 2013. DOI: https://doi.org/10.1016/j.rser.2012.10.048

[19] Elsheniti M.B., Kotb A., Elsamni O., Thermal performance of a heat-pipe evacuated-tube solar collector at high inlet temperatures, *Applied Thermal Engineering*, **154**: 315–325, 2019. DOI: https://doi.org/10.1016/j.applthermaleng.2019.03.106

[20] Roulet C.A., *Measuring Thermal Characteristics of Building Insulation Materials*, Technical Report, Swiss Federal Institute of Technology in Lausanne (EPFL), Lausanne, Switzerland, 2015, DOI: https://doi.org/10.13140/RG.2.2.31730.50881

[21] Hill J., Kusuda T., *Method of Testing for Rating Solar Collectors Based on Thermal Performance*, National Bureau of Standards (NBSIR 74-635), Gaithersburg, MD, USA, 1974, https://doi.org/10.6028/NBS.IR.74-635

[22] Tang R., Gao W., Yu Y., Chen H., Optimal tilt-angles of all-glass evacuated tube solar collectors, *Energy*, **34**(9): 1387–1395, 2009, https://doi.org/10.1016/j.energy.2009.06.014

[23] Sharafeldin M.A., Gróf G., Evacuated tube solar collector performance using CeO_2/water nanofluid, *Journal of Cleaner Production*, **185**: 347–356, 2018. DOI: https://doi.org/10.1016/j.jclepro.2018.03.054

[24] Beck M.P., Yuan Y., Warrier P., Teja A.S., The effect of particle size on the thermal conductivity of alumina nanofluids, *Journal of Nanoparticle Research*, **11**(5): 1129–1136, 2009. DOI: https://doi.org/10.1007/s11051-008-9500-2

[25] Oh D.W., Jain A., Eaton J.K., Goodson K.E., Lee J.K., Thermal conductivity measurement and sedimentation detection of aluminium oxide nanofluids by using the 3ω method, *International Journal of Heat and Fluid Flow*, **29**(5): 1456–1461, 2008. DOI: https://doi.org/10.1016/j.ijheatfluidflow.2008.04.007

PRE-PROOF PUBLICATION

PRE-PROOF PUBLICATION ENGINEERING TRANSACTIONS